

# Thermoelectric transport in $\text{Bi}_2\text{Te}_3/\text{Sb}_2\text{Te}_3$ superlattices

N. F. Hinsche,<sup>1,\*</sup> B. Yu. Yavorsky,<sup>2</sup> M. Gradhand,<sup>3</sup> M. Czerner,<sup>4</sup>  
M. Winkler,<sup>5</sup> J. König,<sup>5</sup> H. Böttner,<sup>5</sup> I. Mertig,<sup>1,6</sup> and P. Zahn<sup>7</sup>

<sup>1</sup>*Institut für Physik, Martin-Luther-Universität Halle-Wittenberg, DE-06099 Halle, Germany*

<sup>2</sup>*Forschungszentrum Karlsruhe, Hermann-von-Helmholtz-Platz 1, 76344 Eggenstein-Leopoldshafen, Germany.*

<sup>3</sup>*H. H. Wills Physics Laboratory, University of Bristol, Bristol BS8 1TH, United Kingdom*

<sup>4</sup>*I. Physikalisches Institut, Justus-Liebig-Universität Gießen, DE-35392 Gießen, Germany*

<sup>5</sup>*Fraunhofer Institut für Physikalische Messtechnik,  
Heidenhofstrasse 8, DE-79110 Freiburg, Germany*

<sup>6</sup>*Max-Planck-Institut für Mikrostrukturphysik, Weinberg 2, DE-06120 Halle, Germany*

<sup>7</sup>*Helmholtz-Zentrum Dresden-Rossendorf, P.O.Box 51 01 19, DE-01314 Dresden, Germany*

(Dated: June 20, 2012)

The thermoelectric transport properties of  $\text{Bi}_2\text{Te}_3/\text{Sb}_2\text{Te}_3$  superlattices are analyzed on the basis of first-principles calculations and semi-classical Boltzmann theory. The anisotropy of the thermoelectric transport under electron and hole-doping was studied in detail for different superlattice periods at changing temperature and charge carrier concentrations. A clear preference for thermoelectric transport under hole-doping, as well as for the in-plane transport direction was found for all superlattice periods. At hole-doping the electrical transport anisotropies remain bulk-like for all investigated systems, while under electron-doping quantum confinement leads to strong suppression of the cross-plane thermoelectric transport at several superlattice periods. In addition, insights on the Lorenz function, the electronic contribution to the thermal conductivity and the resulting figure of merit are given.

PACS numbers: 31.15.A-, 71.15.Mb, 72.20.Pa, 72.20.-i

## I. INTRODUCTION

Solid-state thermoelectric (TE) power generation devices possess the desirable nature of being highly reliable, stable, compact and integrable and have potential applications in waste-heat recovery and outer space explorations. However, while intensively studied in the last decades, poor energy conversion efficiencies below a few percent at room temperature prohibited the triumph of the TE devices as promising alternative energy sources. The conversion performance of a thermoelectric material is quantified by the figure of merit (FOM)

$$ZT = \frac{\sigma S^2}{\kappa_{el} + \kappa_{ph}} T, \quad (1)$$

where  $\sigma$  is the electrical conductivity,  $S$  the thermopower,  $\kappa_{el}$  and  $\kappa_{ph}$  are the electronic and lattice contribution to the thermal conductivity, respectively. From Eq. 1 it is obvious, that a higher  $ZT$  is obtained by decreasing the denominator or by increasing the numerator, the latter being called power factor  $\text{PF} = \sigma S^2$ . While  $\sigma$ ,  $S$ ,  $\kappa_{el}$  and  $\kappa_{ph}$  can individually be tuned by several orders of magnitude, the interdependence between these properties impede high values for the FOM<sup>1,2</sup>.  $\text{Bi}_2\text{Te}_3$ ,  $\text{Sb}_2\text{Te}_3$  and their related alloys dominate the field of thermoelectrics with  $ZT$  around unity from the 1950's through today<sup>3-5</sup>.

The idea of thermoelectric superlattices (SL) allows for concepts, which could enable both, the suppression of the cross-plane thermal conductivity<sup>6-8</sup> and the increase of the electronic power factor<sup>9</sup>. It suggests that cross-plane transport along the direction perpendicular to the artificial interfaces of the SL reduces phonon heat

conduction while maintaining or even enhancing the electron transport<sup>10</sup>. In 2001 a break-through experiment by Venkatasubramanian *et al.* reported a record apparent  $ZT = 2.4$  for p-type  $\text{Bi}_2\text{Te}_3/\text{Sb}_2\text{Te}_3$  and  $ZT = 1.4$  for n-type  $\text{Bi}_2\text{Te}_3/\text{Bi}_2\text{Te}_{2.83}\text{Se}_{0.17}$  superlattices<sup>8,11,12</sup>, although this values have not yet been reproduced to the best of our knowledge.

With the availability of materials with  $ZT \geq 3$  thermoelectric materials could compete with conventional energy conversion methods and new applications could emerge<sup>13</sup>. Beside thermal conductivities below the alloy limit, the investigations of Venkatasubramanian *et al.*<sup>12</sup> found a strong decrease of the mobility anisotropy and the related electronic thermoelectric properties for the SLs at certain periods. This is counter-intuitively, as superlattices are anisotropic by definition and even the telluride bulk materials show intrinsic anisotropic structural and electronic properties<sup>14-18</sup>. While considerable effort was done in experimental research<sup>19-26</sup>, theoretical investigations on  $\text{Bi}_2\text{Te}_3/\text{Sb}_2\text{Te}_3$  SLs are rare. Various available theoretical works concentrate on the electronic structure and transport properties of the bulk materials<sup>17,27-29</sup>, with some of them discussing the influence of strain, which could occur at the SL interfaces<sup>18,30,31</sup>. To our knowledge, only a sole theoretical work discussed the possible transport across such telluride SL structures. Based on density functional theory, Li *et al.*<sup>32</sup> focussed on the calculation of the electronic structure for two distinct  $\text{Bi}_2\text{Te}_3/\text{Sb}_2\text{Te}_3$  SLs, stating changes of the mobility anisotropy estimated from effective masses. To extend this work and to clarify the open questions on the reduced mobility anisotropy and the enhanced thermoelec-

tric efficiency, we are going to discuss in this paper the anisotropic thermoelectric electronic transport of seven different  $\text{Bi}_2\text{Te}_3/\text{Sb}_2\text{Te}_3$  SLs, including the bulk materials, on the basis of density functional theory and semi-classical transport calculations.

For this purpose the paper will be organized as follows. In Sec. II we introduce our first principle electronic structure calculations based on density functional theory and the semi-classical transport calculations based on the solution of the linearized Boltzmann equation. A brief discussion of the obtained band structures, including the dependence of the band gap on different SL periods, is done in section Sec. III. With this, we present in Sec. IV the electronic thermoelectric transport properties, that is electrical conductivity, thermopower and the related power factor, of the  $\text{Bi}_2\text{Te}_3/\text{Sb}_2\text{Te}_3$  SLs at different SL periods with a focus on their directional anisotropies. The discussions cover a broad temperature and doping range and will conclude the bulk materials. Even though only p-type conduction was found in SLs stacked out of pure  $\text{Bi}_2\text{Te}_3$  and  $\text{Sb}_2\text{Te}_3$  n-type conduction will be studied, too, as being possible at appropriate extrinsic doping. For the latter case strong quantum confinement effects were found, which will be discussed in detail in Sec. IV B. To give a clue on possible values for the figure of merit, in Sec. IV C results for the electronic contribution to the thermal conductivity, the Lorenz function as well as existing experimental results for the lattice part of the thermal conductivity will be presented. Most of the discussions are done in a comparative manner considering the experimental findings of Ref. 12.

## II. METHODOLOGY

For both bismuth and antimony telluride, as well as for the composed heterostructures, we used the experimental lattice parameters and relaxed atomic positions<sup>33</sup> as provided for the hexagonal  $\text{Bi}_2\text{Te}_3$  crystal structure with 15 atomic layers. The layered structure itself is composed out of three formula units,  $\text{Te}_1\text{-Bi-Te}_2\text{-Bi-Te}_1$ , often called quintuples. The hexagonal lattice parameters are chosen to be  $a_{\text{BiTe}}^{\text{hex}} = 4.384\text{\AA}$  and  $c_{\text{BiTe}}^{\text{hex}} = 30.487\text{\AA}$  for  $\text{Bi}_2\text{Te}_3$ ,  $\text{Sb}_2\text{Te}_3$  and the  $\text{Bi}_2\text{Te}_3/\text{Sb}_2\text{Te}_3$  SLs, respectively. In fact, the main difference between the lattices of  $\text{Bi}_2\text{Te}_3$  and  $\text{Sb}_2\text{Te}_3$  is a decrease of the in-plane lattice constant with an accompanied decrease in cell volume. So, a change between the two lattice constants can be related to either compressive or tensile in-plane strain. Preceding intense studies revealed that a larger in-plane lattice constant, e.g.  $a_{\text{BiTe}}^{\text{hex}} > a_{\text{SbTe}}^{\text{hex}}$ , is favourable for an enhanced cross-plane TE transport<sup>18,29,34</sup>. For this purpose, the experimental lattice parameters of  $\text{Bi}_2\text{Te}_3$  were chosen for the studied heterostructures. Structural relaxations revealed only minor influences on the bulk electronic structure<sup>29-32</sup> and are beyond the scope of this work. To introduce SLs with different layer peri-

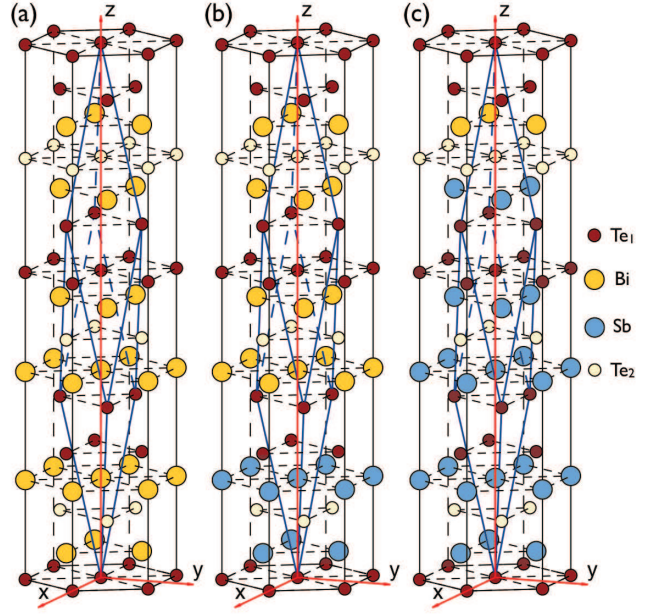


FIG. 1. (color online) Shown are three possible hexagonal unit cells of the  $(\text{Bi}_2\text{Te}_3)_x/(\text{Sb}_2\text{Te}_3)_{1-x}$  superlattices. (a)  $x=1$  which is bulk  $\text{Bi}_2\text{Te}_3$ , (b)  $x=2/3$  and (c)  $x=1/6$ . A concentration  $x=0$  would coincide with bulk  $\text{Sb}_2\text{Te}_3$  in the lattice of  $\text{Bi}_2\text{Te}_3$ .

ods compared to the experiments of Venkatasubramanian *et al.*<sup>12</sup> we subsequently substitute the Bi site by Sb, starting with six Bi sites in hexagonal bulk  $\text{Bi}_2\text{Te}_3$  (see Fig. 1(a)). For instance, substituting two atomic layers of Bi with Sb leads to a  $(\text{Bi}_2\text{Te}_3)_x/(\text{Sb}_2\text{Te}_3)_{1-x}$  SL with  $x = 2/3$ , that is two quintuple  $\text{Bi}_2\text{Te}_3$  and one quintuple  $\text{Sb}_2\text{Te}_3$  (see Fig. 1(b)). The latter case coincides with a  $(20\text{\AA}/10\text{\AA})\text{-(Bi}_2\text{Te}_3/\text{Sb}_2\text{Te}_3)$  superlattice in the experimental notation of Ref. 12.

Our thermoelectric transport calculations are performed in two steps. In a first step, the detailed electronic structure of the  $\text{Bi}_2\text{Te}_3/\text{Sb}_2\text{Te}_3$  SLs were obtained by first principles density functional theory calculations (DFT), as implemented in the fully relativistic screened Korringa-Kohn-Rostoker Greens-function method (KKR)<sup>35</sup>. Within this approach the DIRAC-equation is solved self-consistently and with that spin-orbit-coupling (SOC) is included. Exchange and correlation effects were accounted for by the local density approximation (LDA) parametrized by Vosco, Wilk, and Nusair<sup>36</sup>. Detailed studies on the electronic structure and transport anisotropy of the bulk tellurides  $\text{Bi}_2\text{Te}_3$  and  $\text{Sb}_2\text{Te}_3$  were published before<sup>18,34</sup> and show very good agreement to experimental results and other theoretical findings.

With the well converged results from the first step we obtain the thermoelectric transport properties by solving the linearized Boltzmann equation in relaxation time approximation (RTA) within an in-house developed Boltzmann transport code<sup>37,38</sup>. Boltzmann transport calcula-

tions for thermoelectrics have been carried out for quite a long time and show reliable results for wide- and narrow gap semiconductors<sup>38–42</sup>. Calculations on the electronic structure and TE transport for bulk Bi<sub>2</sub>Te<sub>3</sub><sup>17,31,43,44</sup> and Sb<sub>2</sub>Te<sub>3</sub><sup>28,31,45</sup> were presented before. Here the relaxation time  $\tau$  is assumed to be isotropic and constant with respect to wave vector  $\mathbf{k}$  and energy on the scale of  $k_B T$ . This assumption is widely accepted for degenerate doped semiconductors. Within the RTA, from comparison of the calculated electrical and electronic thermal conductivities (eq. 3 and 4) with experiment it is possible to conclude on the relaxation time. In the following  $\tau$  is set to 10 fs for all bulk and heterostructure systems, regardless of any directional anisotropy or charge carrier dependence. We note, that within RTA for the thermopower  $S$  (eq. 3) the dependence of the transport distribution function (TDF), as introduced in the next paragraph, on the energy is essential. That is, not only the slope of the TDF, moreover the overall functional behaviour of the TDF on the considered energy scale has to change to observe an impact on the thermopower.

Within the RTA the TDF  $\mathcal{L}_{\perp,\parallel}^{(0)}(\mu, 0)$ <sup>46</sup> and with this the generalized conductance moments  $\mathcal{L}_{\perp,\parallel}^{(n)}(\mu, T)$  are defined as

$$\mathcal{L}_{\perp,\parallel}^{(n)}(\mu, T) = \frac{\tau}{(2\pi)^3} \sum_{\nu} \int d^3k \left( v_{k,(\perp,\parallel)}^{\nu} \right)^2 (E_k^{\nu} - \mu)^n \left( -\frac{\partial f(\mu, T)}{\partial E} \right)_{E=E_k^{\nu}}. \quad (2)$$

$E_k^{\nu}$  denotes the band structure of band  $\nu$ ,  $v_k^{\nu}$  the group velocity and  $f(\mu, T)$  the FERMI-DIRAC-distribution.  $v_{k,(\parallel)}^{\nu}$ ,  $v_{k,(\perp)}^{\nu}$  denote the group velocities in the directions in the hexagonal basal plane and perpendicular to it, respectively. Within here the group velocities were obtained as derivatives along the lines of the Blöchl mesh in the whole Brillouin zone (BZ)<sup>34</sup>. The directions of these lines are parallel to the reciprocal space vectors and so the anisotropy of the real lattice is reflected in these vectors. A detailed discussion on implications and difficulties on the numerical determination of the group velocities in highly anisotropic materials was currently published elsewhere<sup>47</sup>. As can be seen straight forwardly, the temperature- and doping-dependent electrical conductivity  $\sigma$  and thermopower  $S$  in the in- and cross-plane directions are defined as

$$\sigma_{\perp,\parallel} = e^2 \mathcal{L}_{\perp,\parallel}^{(0)}(\mu, T) \quad S_{\perp,\parallel} = \frac{1}{eT} \frac{\mathcal{L}_{\perp,\parallel}^{(1)}(\mu, T)}{\mathcal{L}_{\perp,\parallel}^{(0)}(\mu, T)} \quad (3)$$

and the electronic part to the total thermal conductivity accounts to

$$\kappa_{el\perp,\parallel} = \frac{1}{T} (\mathcal{L}_{\perp,\parallel}^{(2)}(\mu, T) - \frac{(\mathcal{L}_{\perp,\parallel}^{(1)}(\mu, T))^2}{\mathcal{L}_{\perp,\parallel}^{(0)}(\mu, T)}). \quad (4)$$

The second term in eq. 4 introduces corrections due to the Peltier heat flow that can occur when bipolar conduction takes place<sup>48</sup>.

The chemical potential  $\mu$  at temperature  $T$  and extrinsic carrier concentration  $N$  is determined by an integration over the density of states (DOS)  $n(E)$

$$N = \int_{-\infty}^{\text{VBM}} dE n(E) [f(\mu, T) - 1] + \int_{\text{CBM}}^{\infty} dE n(E) f(\mu, T)$$

where CBM is the conduction band minimum and VBM is the valence band maximum. The k-space integration of eq. 2 for a system with an intrinsic anisotropic texture, e.g. in rhombohedral and hexagonal structures, is quite challenging. In preceding publications<sup>34,47</sup> we stated on the relevance of adaptive integration methods needed to reach convergence of the energy dependent TDF. Especially in regions close to the band edges, which are evident for transport, the anisotropy of the TDF requires a high density of the k-mesh. Here, convergence tests for the transport properties showed that at least 150 000 k-points in the entire BZ had to be included for sufficient high doping rates ( $N \geq 1 \times 10^{19} \text{ cm}^{-3}$ ), while for energies near the band edges even more than 56 million k-points were required to reach the analytical effective mass values and the corresponding conductivity anisotropies at the band edges.

### III. ELECTRONIC STRUCTURE

In Figs. 1(a)-(g) the electronic bandstructures on the hexagonal high symmetry lines for all (Bi<sub>2</sub>Te<sub>3</sub>)<sub>x</sub>/(Sb<sub>2</sub>Te<sub>3</sub>)<sub>1-x</sub> SLs are shown, starting with (a)  $x = 0$  which is tensile strained bulk Sb<sub>2</sub>Te<sub>3</sub> and ending with (g)  $x = 1$ , which is bulk Bi<sub>2</sub>Te<sub>3</sub>. For the case of (b)  $x = 1/6$ , (d)  $x = 1/2$  and (f)  $x = 5/6$  a further band splitting can be noticed, which stems from the missing space inversion symmetry in these systems and with that the former band degeneracy is lifted. This situation always occurs if the Bi(Sb) sites in each quintuple are not uniformly occupied.

For increasing number of Bi layers in the SLs no drastic change in the band structure topology can be stated. Only slight variations were found for the in-plane band directions. Of stronger impact could be the change of band dispersion which occurs for the lowest lying conduction band in the cross-plane direction  $\Gamma A$ . Here a continuous change of the bands slope is found for increasing amount of Bi layers in the SL. An almost vanishing dispersion and very flat bands in cross-plane direction are found for the SL with  $x = 0.5$ , which is three Bi-like layers and three Sb-like layers. Further amount of Bi layers in the system leads to an increase in the bands slope, while showing different sign compared to bulk Sb<sub>2</sub>Te<sub>3</sub>.

In Fig. 2(h) the calculated band gap in dependence on the superlattice period is shown. Applying an extended tetrahedron method<sup>50,51</sup> and very dense k-mesh's in the BZ, the band gap values were determined within an uncertainty below 1%. While for Sb<sub>2</sub>Te<sub>3</sub> at the experimental lattice parameters, we previously found a di-

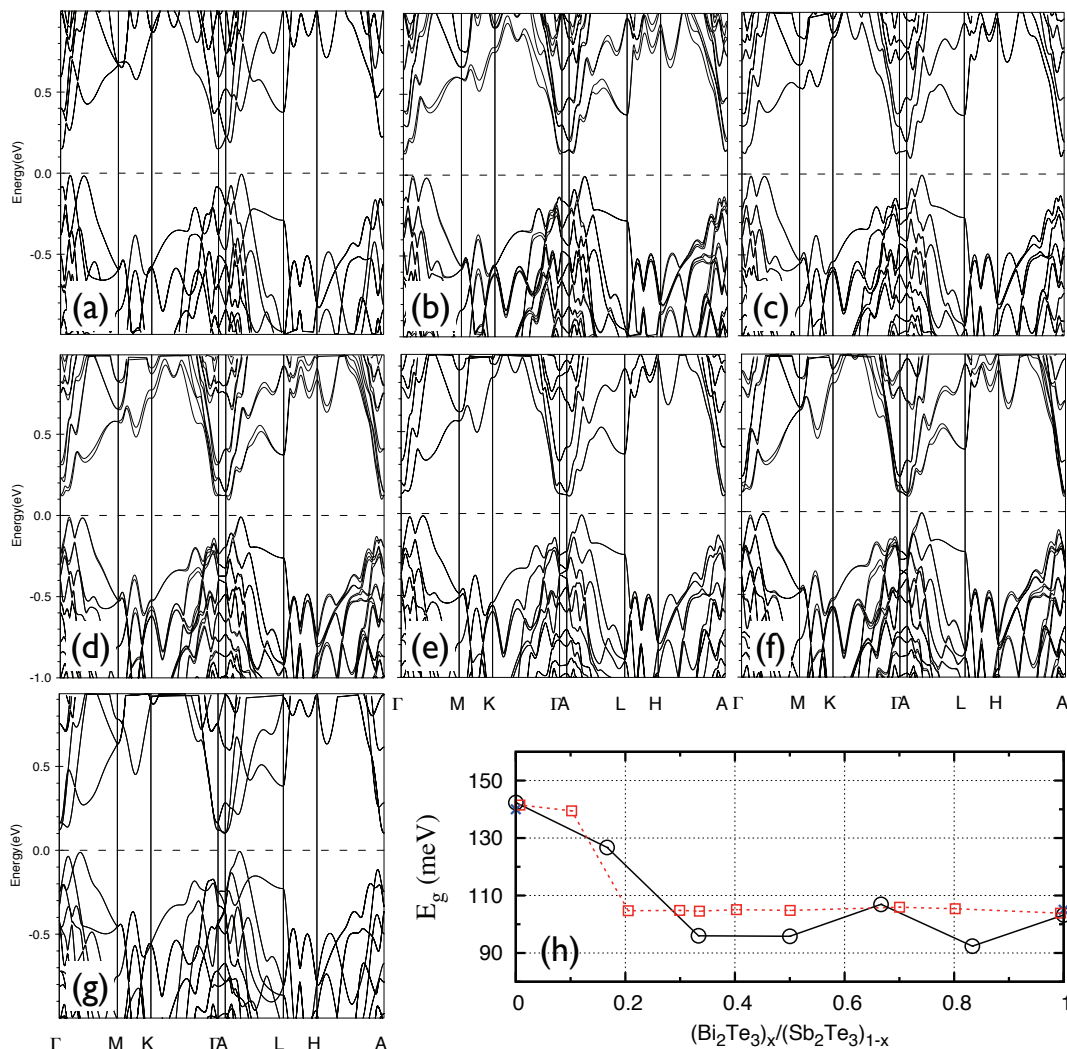


FIG. 2. (color online) Electronic bandstructures for  $(\text{Bi}_2\text{Te}_3)_x/(\text{Sb}_2\text{Te}_3)_{1-x}$  superlattices in the hexagonal unit cell with different superlattice periods. (a)  $x = 0$ , (b)  $x = 1/6$ , (c)  $x = 1/3$ , (d)  $x = 1/2$ , (e)  $x = 2/3$ , (f)  $x = 5/6$  and (g)  $x = 1$ . In (h) black circles show the calculated fundamental energy gap in dependence on the superlattice period. Red squares show experimental findings<sup>49</sup> for  $(\text{Bi}_2\text{Te}_3)_x/(\text{Sb}_2\text{Te}_3)_{1-x}$  alloys, which were linearised to allow for comparison with our LDA results.

rect band gap located at the center of the BZ <sup>34</sup>, an indirect gap of  $E_g = 140$  meV can be stated for the in-plane tensile strained  $\text{Sb}_2\text{Te}_3$ . For  $\text{Bi}_2\text{Te}_3$  as well as for all  $\text{Bi}_2\text{Te}_3/\text{Sb}_2\text{Te}_3$  SLs indirect band gaps are obtained, too. A known difficulty within standard DFT is the general underestimation of the semi-conductors band gaps at zero temperature<sup>52</sup>, as well as the missing temperature dependence of  $E_g(T)$ <sup>53</sup>. For small band gap thermoelectrics, such as  $\text{Bi}_2\text{Te}_3$  and  $\text{Sb}_2\text{Te}_3$ , this could impinge the TE transport. The thermopower might be reduced at high temperature and low doping due to bipolar conduction<sup>17,39</sup>. This effect would be overestimated if the band gap is underestimated. With  $E_g(T)$  being considered for TE bulk materials<sup>17,38</sup> lack of knowledge on the absolute size of the gap, as well as its temperature dependence permits such gap corrections for the strained

bulk materials as well as for the SLs. However, the calculated bulk band gap of  $E_g = 105$  meV for unstrained bulk  $\text{Bi}_2\text{Te}_3$  is in better agreement with the experimental value of  $E_g = 130$  meV<sup>49</sup>, than for unstrained  $\text{Sb}_2\text{Te}_3$  where a calculated value of  $E_g = 90$  meV faces experimental values between  $E_g = 150 - 230$  meV<sup>49,54</sup>. As is well known,  $\text{Bi}_2\text{Te}_3$  and  $\text{Sb}_2\text{Te}_3$  exhibit band inversions at certain areas in the BZ<sup>55</sup>. Within LDA the strength of band inversion is most likely underestimated<sup>56</sup>. At a given band inversion the strength of the spin orbit interaction then controls the size of the band gap. Fortunately, overestimated SOC effects and underestimated band inversion tend to cancel each other leading to good results for the band gap size and wave function character.

As a lack of data, we can only compare the Bi<sub>2</sub>Te<sub>3</sub>/Sb<sub>2</sub>Te<sub>3</sub> SL with  $x = 1/3$  (see Fig. 2(c)) with pre-



vious results of Li *et al.*<sup>32</sup>. While they applied a full-potential Linearized Augmented Plane Wave (FLAPW) method and treated spin-orbit coupling as a second order perturbation, the results on the bands topology are in very good agreement. However, our band gap is substantially larger with  $E_g = 95$  meV neglecting any structural relaxations, compared to their value of  $E_g = 27$  meV.

## IV. THERMOELECTRIC TRANSPORT

### A. Effects of superlattice period composition

With knowledge on the electronic structure, we are now able to calculate the desired thermoelectric transport properties of the  $\text{Bi}_2\text{Te}_3/\text{Sb}_2\text{Te}_3$  SLs. As a starting point the in-plane transport properties at room temperature for the electron doped (cf. Figs. 3(a)-(c)) and hole doped (cf. Figs. 3(d)-(f)) heterostructures are chosen, while afterwards the anisotropy referring to the transport in cross-plane direction is discussed in detail. Preliminary studies revealed the optimal charge carrier concentration for the SLs to be in the range of  $3 - 6 \times 10^{19} \text{ cm}^{-3}$ <sup>18</sup>. For the sake of clarity results are presented for three relevant charge carrier concentrations of 3, 6 and  $9 \times 10^{19} \text{ cm}^{-3}$  (cf. solid, dashed and dotted lines in Fig. 3, respectively).

Under electron doping (cf. Fig. 3(a)) a decrease of the in-plane electrical conductivity for the superlattices compared to the bulk materials is found. This decrease is more pronounced at higher charge carrier concentrations, while only slightly being dependent on the SL period. Despite taking into account an isotropic and constant relaxation time  $\tau = 10$  fs, we find very good agreement with experiment<sup>57,58</sup> for bulk  $\text{Bi}_2\text{Te}_3$  with  $\sigma_{\parallel} = 1030 (\Omega\text{cm})^{-1}$  at  $N = 3 \times 10^{19} \text{ cm}^{-3}$ .

The absolute value of the n-type in-plane thermopower is shown in Fig. 3(b). At a carrier concentration of  $N = 3 \times 10^{19} \text{ cm}^{-3}$  a higher amount of  $\text{Bi}_2\text{Te}_3$  in the superlattices leads to a monotonically increase in the thermopower from  $S_{\parallel} = 103 \mu\text{V/K}$  (bulk  $\text{Sb}_2\text{Te}_3$ ) to  $S_{\parallel} = 141 \mu\text{V/K}$  (bulk  $\text{Bi}_2\text{Te}_3$ ), while showing a dip at a composition of  $x = 2/6$  with  $S_{\parallel}$  below  $100 \mu\text{V/K}$ . The latter anomaly is linked to confinement effects and is discussed in detail in Sec. IV B. This overall behaviour of  $S_{\parallel}$  is retained for higher charge carrier concentrations at reasonable smaller absolute values. Assembling the previous results, the power factor  $\text{PF}_{\parallel}$  under relevant electron doping is shown in Fig. 3(c). Clearly, the reduction of in-plane electrical conductivity  $\sigma_{\parallel}$ , as well as the dip of  $S_{\parallel}$  at a SL period of  $x = 2/6$  lead to a minimal power factor of about  $4 \mu\text{W/cmK}^2$  at the named SL period. We find  $\text{PF}_{\parallel}$  for the SLs always to be smaller than expected from an interpolation of the bulk absolute values. Furthermore due to compensation effects of  $\sigma_{\parallel}$  and  $S_{\parallel}$  the dependence on the amount of doping is less drastically for  $\text{PF}_{\parallel}$  than for its constituents.

The best power factor was found for bulk  $\text{Bi}_2\text{Te}_3$  to be  $\text{PF}_{\parallel} = 21 \mu\text{W/cmK}^2$ , while experimentally thin films and single crystals show  $\text{PF}_{\parallel} = 8 - 27 \mu\text{W/cmK}^2$  and  $\text{PF}_{\parallel} = 45 \mu\text{W/cmK}^2$ , respectively<sup>25,59</sup>. We note here, that in experiment n-type conduction was only apparent for  $\text{Bi}_2\text{Te}_3/\text{Bi}_2\text{Te}_{2.83}\text{Se}_{0.17}$ -SL. Nevertheless, to get more insight the physical mechanisms in thermoelectric SL transport, n-type transport in  $\text{Bi}_2\text{Te}_3/\text{Sb}_2\text{Te}_3$  SLs should be of enhanced interest, too.

Highest power factors and FOM were experimentally found for p-type  $\text{Bi}_2\text{Te}_3/\text{Sb}_2\text{Te}_3$  SLs. The preference for hole conduction is dedicated to the large inherent defects introduced by the  $\text{Sb}_2\text{Te}_3$  layers. In Figs. 3(d)-(f) the in-plane thermoelectric transport properties under hole doping are displayed in the same manner as done before. Compared to the electron doped case (cf. Fig. 3(a)) the hole electrical conductivity  $\sigma_{\parallel}$  is higher at the same charge carrier concentration. Furthermore almost no decrease of  $\sigma_{\parallel}$  could be found for the SLs, while this is more visible at lower charge carrier concentrations. For the in-plane thermopower the values at different superlattice compositions are again only slightly suppressed compared to the bulk systems. For a  $(\text{Bi}_2\text{Te}_3)_x/(\text{Sb}_2\text{Te}_3)_{1-x}$  SL at  $x = 3/6$  we state  $S_{\parallel} = 149 \mu\text{V/K}$ , while  $S_{\parallel} = 154 \mu\text{V/K}$  and  $S_{\parallel} = 150 \mu\text{V/K}$  were found for bulk  $\text{Sb}_2\text{Te}_3$  and  $\text{Bi}_2\text{Te}_3$  at the lowest charge carrier concentration, respectively. This negative bending of the thermopower at different superlattice periods is reflected and enhanced for  $\text{PF}_{\parallel}$ . From Fig. 3(f) it can be seen, that the in-plane power factor  $\text{PF}_{\parallel}$  for the various superlattice is decreased compared to the bulk materials. However, the largest suppression ( $x = 2/6$  and  $x = 3/6$ ) is found to be about 20% compared to the bulk values, but still offers thermoelectric feasible values about  $\text{PF}_{\parallel} = 30 \mu\text{W/cmK}^2$ .

To give a reference, in Table I the calculated in-plane thermoelectric properties are compared to experimental results. In the original work of Venkatasubramanian *et al.*<sup>12</sup> very large values of  $\sigma_{\parallel}$  and  $S_{\parallel}$  result in a huge power factor  $\text{PF}_{\parallel}$  about  $72 \mu\text{W/cmK}^2$  at room temperature<sup>60</sup>. These reported values are way larger than found for bulk or thin film  $\text{Bi}_2\text{Te}_3$ ,  $\text{Sb}_2\text{Te}_3$  or their related alloys<sup>25</sup>. However, in a more recent study Winkler *et al.*<sup>26</sup> reported values for the in-plane electrical conductivity and thermopower of a comparable  $(\text{Bi}_{0.2}\text{Sb}_{0.8})_2\text{Te}_3/\text{Sb}_2\text{Te}_3$  sputtered SL (cf. Table I), which are in very good agreement to our theoretical calculations and combine to an in-plane power factor  $\text{PF}_{\parallel}$  above  $30 \mu\text{W/cmK}^2$ . This is similar to values for bulk single crystals with comparable compositions. In contrast to the original experiments<sup>12,61</sup>, which used low-temperature metal-organic chemical vapor deposition (MOCVD), Winkler *et al.* applied the concept of “nano-alloying”<sup>21</sup>. Here the elemental layers Bi, Sb, and Te are deposited by sputtering and subsequently annealed to induce interdiffusion and a solid-state reaction to form the SLs. The pronounced periodicity and c-orientation of the SLs have been demonstrated by secondary ion mass spectrometry (SIMS) and X-ray diffrac-

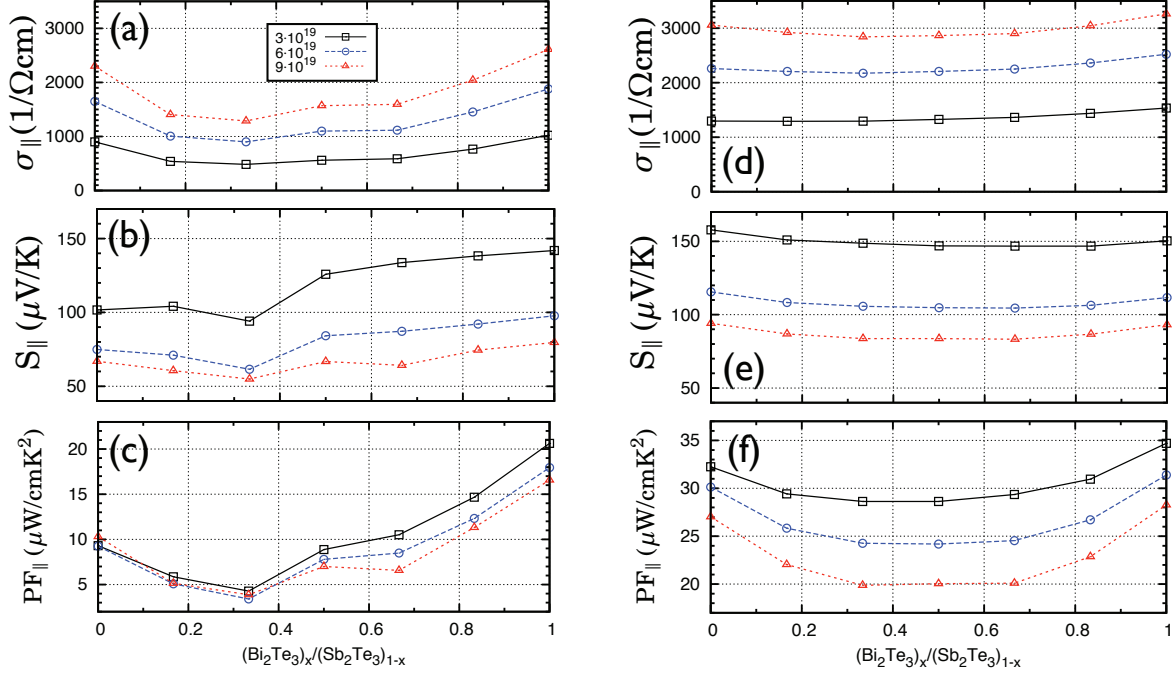


FIG. 3. (color online) Absolute values of in-plane thermoelectric transport properties for  $(\text{Bi}_2\text{Te}_3)_x/(\text{Sb}_2\text{Te}_3)_{1-x}$  superlattices in dependence on the superlattice period. Shown are (a),(d) electrical conductivity  $\sigma_{\parallel}$  (b),(e) thermopower  $S_{\parallel}$  and (c),(f) power factor  $\text{PF}_{\parallel}$ . The temperature is fixed to 300 K and results for three different charge carrier concentrations (in units of  $\text{cm}^{-3}$ ) are stated. (a), (b), (c) refer to electron doping, while (d), (e), (f) refer to hole doping.

TABLE I. Theoretical and experimental in-plane thermoelectric properties of p-type  $(\text{Bi}_2\text{Te}_3)_x/(\text{Sb}_2\text{Te}_3)_{1-x}$  SLs at room temperature. The materials composition amounts in all considered systems to about  $x = 1/6$ . See text for additional details.

| N<br>( $10^{19} \text{ cm}^{-3}$ ) | $\sigma_{\parallel}$<br>( $\Omega\text{cm}$ ) $^{-1}$ | $S_{\parallel}$<br>( $\mu\text{V/K}$ ) | $\text{PF}_{\parallel}$<br>( $\mu\text{W/cmK}^2$ ) | Ref.              |
|------------------------------------|---|--|--|-------------------|
| 3.0                                | 1300  | 151                                    | 30   | this work         |
| 3.1                                | 1818  | $\sim 200$                             | $\sim 72$  | [12, 61–63]       |
| 3.2                                | 761 – 1160  | 172 – 189                              | 27 – 34  | [26] <sup>a</sup> |
| 5.8                                | 3050  | 115                                    | 40   | [64] <sup>b</sup> |

<sup>a</sup> sputtered  $(\text{Bi}_{0.2}\text{Sb}_{0.8})_2\text{Te}_3/\text{Sb}_2\text{Te}_3$  SL

<sup>b</sup>  $(\text{Bi}_x\text{Sb}_{1-x})_2\text{Te}_3$  mixed crystal

tion (XRD), respectively.

While up to now we considered only in-plane transport, in the following the cross-plane transport of the superlattices will be discussed. The transport direction is therefore along the SL direction, perpendicular to the hexagonal basal plane of the bulk materials. In detail the directional anisotropy of the transport properties at room temperature are depicted in Figs. 4(a)-(c) and (d)-(f), for electron and hole doping, respectively. To get the absolute values for cross-plane transport, the in-plane values previously shown in Fig. 3 should be divided by the

anisotropies presented hereinafter. Anisotropies larger than unity represent suppressed thermoelectric transport in cross-plane direction and are therefore less desirable. As has been previously proven by experiment<sup>14–16,44,57</sup> and theory<sup>17,18,27,28</sup>, already the bulk thermoelectrics  $\text{Bi}_2\text{Te}_3$  and  $\text{Sb}_2\text{Te}_3$  show large anisotropies for the electrical conductivity, thermopower and the related power factor.

For a sense of purpose, the thermoelectric transport anisotropies under influence of hole doping will be considered first. In Fig. 4(d) the anisotropy ratio of the electrical conductivity for various SL periods is illustrated at a temperature of 300 K. The anisotropy  $\sigma_{\parallel}/\sigma_{\perp}$  develops smoothly and monotonously between the bulk limits of  $\sigma_{\parallel}/\sigma_{\perp} = 2.7$  and about  $\sigma_{\parallel}/\sigma_{\perp} = 5 - 6$  for bulk  $\text{Sb}_2\text{Te}_3$  and  $\text{Bi}_2\text{Te}_3$ , respectively. With increasing amount of  $\text{Bi}_2\text{Te}_3$  in the superlattices the dependence of  $\sigma_{\parallel}/\sigma_{\perp}$  on the charge carrier concentration is more pronounced. This is in accordance to previous findings for the bulk materials<sup>18</sup>. For the thermopower anisotropy  $S_{\parallel}/S_{\perp}$  this picture holds, too. While for  $\text{Sb}_2\text{Te}_3$  only a slight anisotropy of about  $S_{\parallel}/S_{\perp} = 0.9$  is found, the asymmetry increases for increasing amount of Bi in the SLs, saturating to about  $S_{\parallel}/S_{\perp} = 0.75$  for bulk  $\text{Bi}_2\text{Te}_3$ . The fact of the cross-plane thermopower being enhanced compared to the in-plane part is well known for the two bulk tellurides and compensates somewhat the high electri-

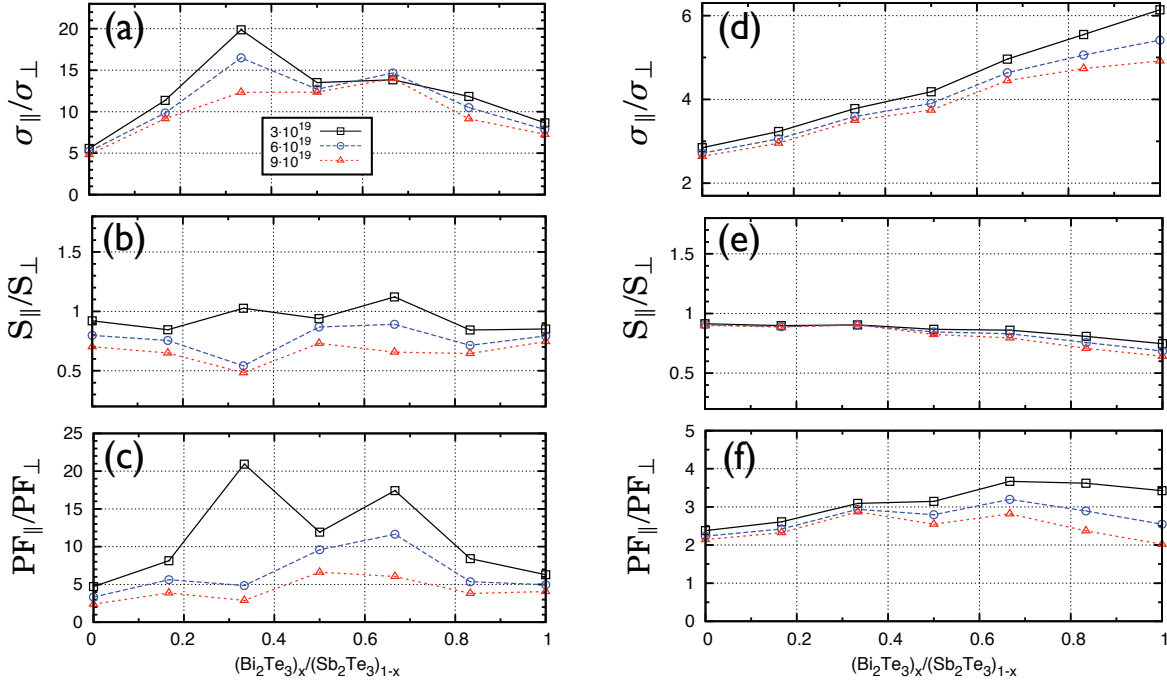


FIG. 4. (color online) Directional anisotropies of thermoelectric transport properties for  $(\text{Bi}_2\text{Te}_3)_x/(\text{Sb}_2\text{Te}_3)_{1-x}$  superlattices in dependence on the superlattice period. Shown are (a),(d) electrical conductivity ratio  $\sigma_{\parallel}/\sigma_{\perp}$  (b),(e) thermopower ratio  $S_{\parallel}/S_{\perp}$  and (c),(f) power factor ratio  $\text{PF}_{\parallel}/\text{PF}_{\perp}$ . The temperature is fixed to 300 K and results for three different charge carrier concentrations (in units of  $\text{cm}^{-3}$ ) are compared. (a), (b), (c) refer to electron doping, while (d), (e) and (f) refer to hole doping.

cal conductivity anisotropy  $\sigma_{\parallel}/\sigma_{\perp}$  to result in a less suppressed cross-plane power factor<sup>18,44</sup>. The anisotropy for the latter is shown in Fig. 4(f). Obviously,  $\text{PF}_{\parallel}/\text{PF}_{\perp}$  is well above unity for all systems indicating a less preferred cross-plane electronic transport. Compared to the bulk values of  $\text{PF}_{\parallel}/\text{PF}_{\perp} = 2.2$  and  $\text{PF}_{\parallel}/\text{PF}_{\perp} = 2 - 3.5$  for bulk  $\text{Sb}_2\text{Te}_3$  and  $\text{Bi}_2\text{Te}_3$ , respectively, the power factor anisotropy is only slightly larger for the SLs with different periods. As an example, for  $x = 1/6$ , which refers to a  $5\text{\AA}/25\text{\AA}$   $\text{Bi}_2\text{Te}_3/\text{Sb}_2\text{Te}_3$  SL, the cross-plane power flow  $\text{PF}_{\parallel}/\text{PF}_{\perp}$  is only suppressed by 13% with respect to bulk  $\text{Sb}_2\text{Te}_3$ , while being enhanced by 26% compared to bulk  $\text{Bi}_2\text{Te}_3$  at the optimal charge carrier concentration of  $N = 3 \times 10^{19} \text{ cm}^{-3}$ . For the thermal conductivity in the SLs a suppression compared to bulk and the related alloys by about a factor of five is expected<sup>8,12</sup>. This would clearly lead to a benefit for the resulting FOM in comparison to bulk, which is discussed more in detail in sec. IV C. However, we want to mention, that in the experiments of Venkatasubramanian *et al.* a further decrease in the electrical conductivity anisotropy was found for thin SLs at various SL periods<sup>12</sup>. It was stated that  $\sigma_{\parallel}/\sigma_{\perp}$  under hole doping is about 0.8 – 1.4 for the  $\text{Bi}_2\text{Te}_3/\text{Sb}_2\text{Te}_3$  SLs at different SL periods and therefore electrical cross-plane transport is strongly improved compared to bulk. Our calculations do not show such a trend.

In Fig. 4(a) the electrical conductivity anisotropy

$\sigma_{\parallel}/\sigma_{\perp}$  under electron doping is shown. Bulk  $\text{Bi}_2\text{Te}_3$  and bulk  $\text{Sb}_2\text{Te}_3$  show anisotropies around  $\sigma_{\parallel}/\sigma_{\perp} = 8$  and  $\sigma_{\parallel}/\sigma_{\perp} = 5$ , respectively, in good agreement to earlier studies<sup>18</sup>. One easily recognizes the anisotropy ratios to be larger than expected from the two bulk limits, while obtaining substantially large values of about  $\sigma_{\parallel}/\sigma_{\perp} = 20$  at  $N = 3 \times 10^{19} \text{ cm}^{-3}$  for a SL period of  $x = 2/6$ , that is a  $10\text{\AA}/20\text{\AA}$   $\text{Bi}_2\text{Te}_3/\text{Sb}_2\text{Te}_3$  SL, or one quintuple of  $\text{Bi}_2\text{Te}_3$  and two quintuples of  $\text{Sb}_2\text{Te}_3$ . For the considered case the anisotropy strongly depends on the amount of doping, while decreasing rapidly at increased charge carrier concentration, but still reaching  $\sigma_{\parallel}/\sigma_{\perp} \geq 10$  at  $N = 9 \times 10^{19} \text{ cm}^{-3}$ . At the same time the thermopower anisotropy shows a clear cross-plane preference at  $S_{\parallel}/S_{\perp} \approx 0.5$ . Nevertheless, the resulting power factor anisotropy shows disappointing high values of about  $\text{PF}_{\parallel}/\text{PF}_{\perp} \gg 5$  for the distinct SLs, while even showing  $\text{PF}_{\parallel}/\text{PF}_{\perp}$  about 20 for the SL at a composition of  $x = 2/6$ . The suppressed cross-plane thermoelectric transport can clearly be linked to the large electrical conductivity anisotropies found for the n-type  $\text{Bi}_2\text{Te}_3/\text{Sb}_2\text{Te}_3$  SLs. In the following we want to emphasize, that the latter are related to quantum well effects in the conduction band, which are evoked by a conduction band offset between  $\text{Bi}_2\text{Te}_3$  and  $\text{Sb}_2\text{Te}_3$  in the SLs.





ature in Figure 6 the temperature dependence of the in-plane and cross-plane thermopower and power factor are presented at a electron/hole charge carrier concentration of  $N = 3 \times 10^{19} \text{ cm}^{-3}$ . The p-type thermopower shows only moderate dependencies on the SL period at all temperatures with the anisotropy slightly favouring the cross-plane part  $S_{\perp}$ . Under electron doping the dependence of the thermopower on the SL period is more pronounced, which can to some amount be assigned to the quantum well effects which occur in the conduction band. At higher temperatures the thermopowers anisotropy is distinct larger. The latter was shown before for the bulk materials<sup>18</sup>. Due to the fact of the thermopower, as well as the electrical conductivity being clearly smaller under electron doping than hole doping (cf. Figure 3) we find the largest values of PF for the p-type SLs. Here the largest was found to be  $\text{PF}_{\parallel} = 42 \mu\text{W}/\text{cmK}^2$  at 500 K for  $(\text{Bi}_2\text{Te}_3)_x/(\text{Sb}_2\text{Te}_3)_{1-x}$  SL with  $x = 1/6$ . For bulk  $\text{Bi}_2\text{Te}_3$  and  $\text{Sb}_2\text{Te}_3$  we state maximum  $\text{PF}_{\parallel} = 44 \mu\text{W}/\text{cmK}^2$  and  $49 \mu\text{W}/\text{cmK}^2$  at 400 K and 550 K, respectively. Due to previously discussed conductivity anisotropy  $\sigma_{\parallel}/\sigma_{\perp}$ , the cross-plane PF is strongly suppressed and the maxima are shifted to higher temperatures.

### C. Towards figure of merit

With the electronic transport properties discussed in the previous sections, we are now going to focus on the electronic and lattice part contribution to the thermal conductivity  $\kappa_{el} + \kappa_{ph}$  to give some estimations on the FOM. As has been stated before, the main benefit from a superlattice structure for the FOM is expected from a reduction of the cross-plane thermal conductivity at retained electronic transport properties. Today, the reduction of the cross-plane lattice thermal conductivity in thermoelectric superlattices has been widely and successfully proven<sup>72–75</sup>.

In the past thermal conductivity reduction in crystalline or polycrystalline bulk thermoelectric materials was traditionally achieved by alloying. However, one reaches the so-called alloy limit of thermal conductivity, which has been difficult to surpass by nanostructuring<sup>2</sup>.

Nevertheless, for  $\text{Bi}_2\text{Te}_3/\text{Sb}_2\text{Te}_3$  SLs cross-plane lattice thermal conductivities of  $\kappa_{ph} = 0.22 \text{ W}/\text{mK}$  were reported for certain SL periods, which is a factor of two below the alloy limit<sup>8</sup>. It is obvious, that at thermoelectric relevant charge carrier concentrations and temperature ranges, the electronic contribution  $\kappa_{el}$  can be in the same order of magnitude.

Therefore Figure 7 shows the room temperature doping dependent electronic part of the thermal conductivity, in the in-plane (thick dashed lines, right scale) and cross-plane direction (thin dashed lines, right scale), for bulk  $\text{Bi}_2\text{Te}_3$ , to give insight in the principle dependencies. Furthermore, the Lorenz function defined via Eqs. 3 and 4 as  $L_{\perp,\parallel} = \kappa_{el\perp,\parallel} \cdot (\sigma_{\perp,\parallel} \cdot T)^{-1}$  is shown for the

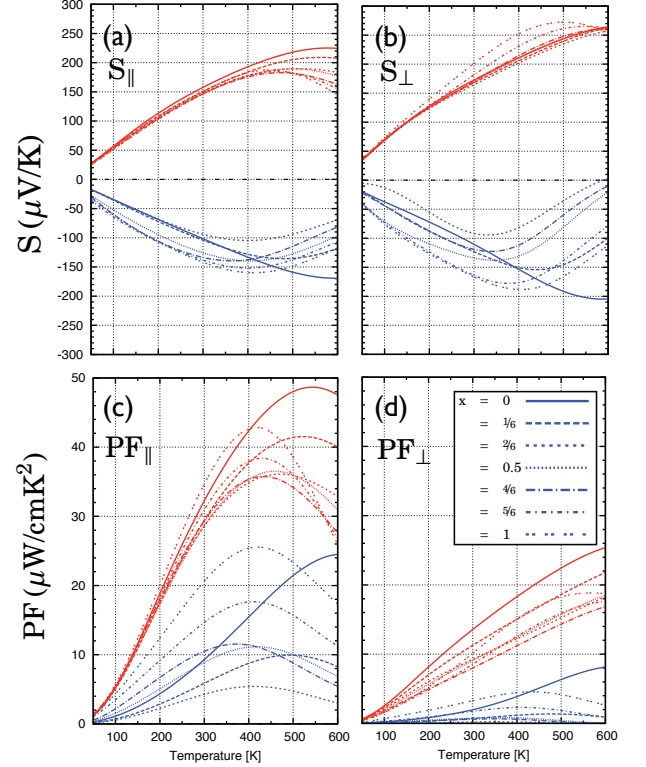


FIG. 6. (color online) Temperature dependence of thermoelectric transport properties for  $(\text{Bi}_2\text{Te}_3)_x/(\text{Sb}_2\text{Te}_3)_{1-x}$  superlattices. Shown are (a) in-plane thermopower  $S_{\parallel}$  and (b) cross-plane thermopower  $S_{\perp}$ , as well as the corresponding power factors (c)  $\text{PF}_{\parallel}$  in the in-plane and (d)  $\text{PF}_{\perp}$  in the cross-plane direction. The charge carrier concentration is fixed to  $N = 3 \times 10^{19} \text{ cm}^{-3}$  and different line types correspond to different superlattice periods. Blue lines refer to electron doping, while red lines refer to hole doping.

in-plane (thick solid line, left scale and color code) and cross-plane part (thin solid line, left scale), respectively. As can be seen,  $\kappa_{el}$  minimizes for energies near the band edges. Here, at  $N \approx 3 \times 10^{18} \text{ cm}^{-3}$ , the thermopower  $S$  maximizes at appropriate values for the electrical conductivity  $\sigma$ , hence the second term in Eq. 4 increases leading to small values for  $\kappa_{el}$ . At small intrinsic charge carrier concentrations, the chemical potential shifts into the gap and the total thermopower is strongly reduced due to bipolar diffusion. This leads to an enhanced contribution to the electrical thermal conductivity at intrinsic charge carrier concentrations and is known as the bipolar thermodiffusion effect<sup>76–78</sup>. At charge carrier concentrations of  $N = 3 \times 10^{19} \text{ cm}^{-3}$  we find  $\kappa_{el\parallel}$  to be about  $0.6 - 0.8 \text{ W}/\text{mK}$  for n/p-type bulk  $\text{Bi}_2\text{Te}_3$  in very good agreement with experimental (cf. green, open circles in Fig. 7) and theoretical results<sup>17,23,79</sup>. The cross-plane component of  $\kappa_{el}$  is substantially smaller, especially for n-type conduction, reflecting here the electrical conductivity anisotropy discussed earlier. The bipolar thermod-

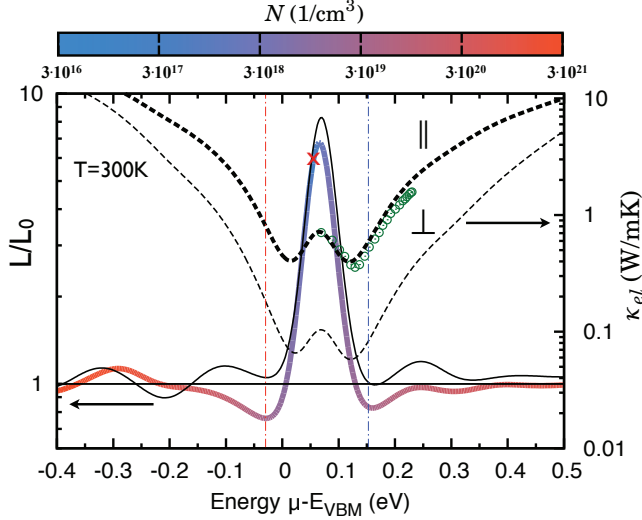


FIG. 7. (color online) Lorenz function  $L$  (solid lines, ref. to left scale) and electronic contribution  $\kappa_{el}$  to the total thermal conductivity (dashed lines, ref. to the right scale) in dependence on position of the chemical potential  $\mu$  for bulk  $\text{Bi}_2\text{Te}_3$  for the in-plane (thick lines) and cross-plane (thin lines) transport direction. The Lorenz function is related to the metallic limit  $L_0 = 2.44 \times 10^{-8} \text{ W}\Omega/\text{K}^2$ . Plotted on to the Lorenz function in the in-plane direction is a color code referring to the charge carrier concentration given by Eq. 5. The red cross emphasizes the change from n to p doping, respectively. The temperature was fixed to 300 K. Thin vertical dash-dotted lines emphasize the position of the chemical potential for a charge carrier concentration of  $N = 3 \times 10^{19} \text{ cm}^{-3}$  under n and p doping (blue and red line, respectively). The CBM is located at 0.105 eV. Green open circles show experimental values from Ref.<sup>76</sup> for  $\kappa_{el,||}$  for an n-type  $\text{Bi}_2\text{Te}_3$  single crystal.

iffusion effect is furthermore responsible for the suppression of the Lorenz function to values below the metallic limit  $L_0$  ( $L_0 = 2.44 \times 10^{-8} \text{ W}\Omega/\text{K}^2$ ) for values of the chemical potential near the band edges (cf. Figure 7 solid lines, right scale). At optimal charge carrier concentrations of  $N = 3 \times 10^{19} \text{ cm}^{-3}$   $L_{||} \approx 0.7L_0$  under hole doping (red dashed dotted lines) and  $L_{||} \approx 0.8L_0$  under electron doping (blue dashed dotted lines) can be found. For the cross-plane Lorenz function  $L_{\perp} \approx L_0$  is stated at the same amount of n/p-type doping. Reaching the intrinsic doping regime the Lorenz function reaches substantially large values of  $L_{||} \approx 6.5L_0$  and  $L_{\perp} \approx 8L_0$ . Such a behaviour has been described in literature<sup>17,80</sup> and can have consequences for the determination of the thermal conductivity. The Lorenz factor is generally used to separate  $\kappa_{el}$  and  $\kappa_{ph}$ . At thermoelectric advisable charge carrier concentrations applying the metallic value  $L_0$  to determine the lattice thermal conductivity could lead to an overestimation of the electronic thermal conductivity, and consequently to underestimation of the lattice contribution. The Lorenz function of thermoelectric heterostructures can show further anomalies which are dis-

cussed in detail in a forthcoming publication<sup>81</sup>.

Experimental findings for the lattice part  $\kappa_{ph}$  of the thermal conductivity are added to the calculated electronic contribution  $\kappa_{el}$  to present some estimations on the cross-plane FOM  $ZT_{\perp}$ . In particular  $\kappa_{ph,\perp} = 1.05 \text{ W/mK}$ ,  $\kappa_{ph,\perp} = 0.96 \text{ W/mK}$  and  $\kappa_{ph,\perp} = 0.22 \text{ W/mK}$  at room temperature were used for bulk  $\text{Bi}_2\text{Te}_3$ ,  $\text{Sb}_2\text{Te}_3$  and the  $\text{Bi}_2\text{Te}_3/\text{Sb}_2\text{Te}_3$  SLs<sup>8</sup>, respectively<sup>82</sup>.

Recently Winkler *et al.*<sup>26</sup> measured for a p-type  $(\text{Bi}_{0.2}\text{Sb}_{0.8})_2\text{Te}_3/\text{Sb}_2\text{Te}_3$  SL the total cross-plane thermal conductivity  $\kappa_{\perp}$  to be about  $0.45 - 0.65 \text{ W/mK}$  for different annealing temperatures. The values were obtained within a time-domain thermal reflectance (TDTR) measurement and are in very good agreement to our calculations, which are displayed in Figure 8(c). Compared to the original experiments by Venkatasubramanian *et al.*<sup>12</sup>, the values of the total cross-plane thermal conductivity are smaller. This stems to a large extent from the fact that a strong electrical conductivity anisotropy  $\sigma_{||}/\sigma_{\perp}$  is apparent and not vanishing to  $\sigma_{||}/\sigma_{\perp} \sim 1$  as proposed in Ref. 12. Hence not only  $\sigma_{\perp}$  but also  $\kappa_{el,\perp}$  is noticeably suppressed. Furthermore in Refs. 8 and 12 it was suggested, that mirror-like SL interfaces lead to potential reflection effects and reduce  $\kappa_{ph,\perp}$  very efficiently. Beside that, Touzelbaev *et al.*<sup>24</sup> showed that an existing interface roughness will additionally decrease  $\kappa_{ph,\perp}$ . Beside the nano-crystallinity of the samples, such an additional interface roughness is most likely provided by interdiffusion effects at the interfaces introduced by the growth of  $\text{Bi}_2\text{Te}_3/\text{Sb}_2\text{Te}_3$  SLs within the concept of “nano-alloying”<sup>21,26</sup>.

In Figure 8 the room-temperature cross-plane properties of the total thermal conductivity and the related cross-plane part of the FOM are shown, for electron (a),(b) and hole doping (c),(d), respectively. As could be expected the strong quantum well effects in the conduction band lead to quite small values for  $ZT_{\perp} \leq 0.2$  under electron doping. Here a reduction of the SL total thermal conductivity of about a factor 5-6 compared to bulk is impeded by an accompanied reduction of  $\text{PF}_{\perp}$  by a factor of 10-20 (cf. Figure 4(c)). Thus no benefit for the FOM in the cross-plane direction can be revealed under electron doping. At hole doping the situation is more advantageous. Beside the total thermal conductivity (cf. Figure 8(c) and Figure 7) being somewhat larger than under electron doping, the electronic transport properties remain bulk-like for all SL periods (cf. Figure 4(f)) and hence an enhancement for  $ZT_{\perp}$  by a factor of 2-3 can be achieved under hole doping of  $N = 3 \times 10^{19} \text{ cm}^{-3}$ . We state values  $ZT_{\perp} \approx 0.7 - 0.9$  for different SL periods, while an higher amount of  $\text{Sb}_2\text{Te}_3$  in the SL leads to larger values for ZT, despite no distinct influence of the SL period on the FOM could be found. As a supplement experimental data<sup>64</sup> for  $\kappa_{\perp}$  and  $ZT_{\perp}$  of the mixed single crystal series  $(\text{Bi}_x\text{Sb}_{1-x})_2\text{Te}_3$  is shown as green downward triangles in Figure 8(c) and (d). The hole doping varied steadily between  $N = 1 \times 10^{19} \text{ cm}^{-3}$  for  $\text{Bi}_2\text{Te}_3$  to

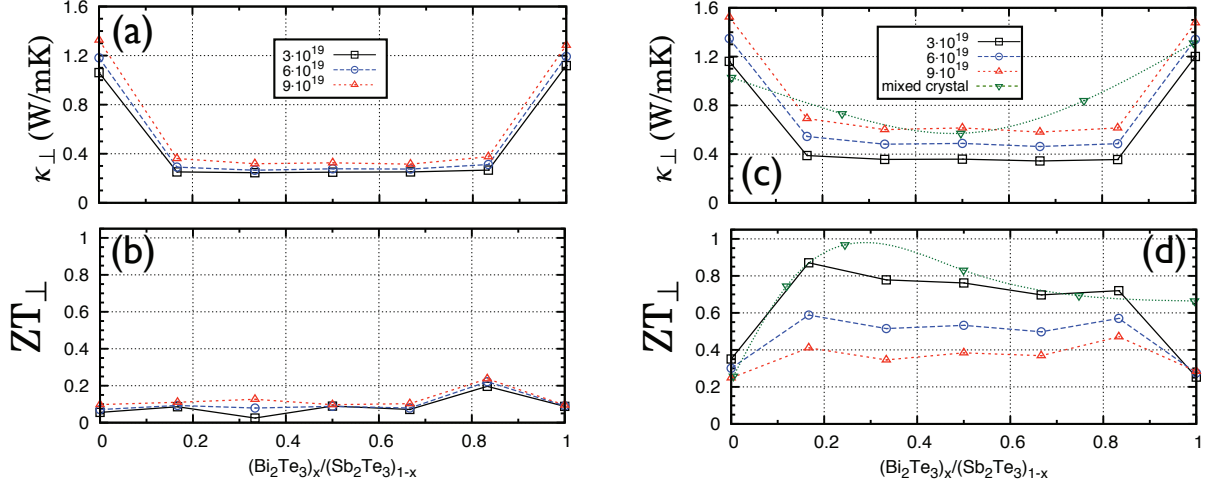


FIG. 8. (color online) Absolute values of cross-plane thermoelectric transport properties for  $(\text{Bi}_2\text{Te}_3)_x/(\text{Sb}_2\text{Te}_3)_{1-x}$  superlattices in dependence on the superlattice period. Shown are (a),(c) the total thermal conductivity  $\kappa_{el} + \kappa_{ph}$  and (b),(d) the cross-plane figure of merit  $ZT_{\perp}$ . The temperature is fixed to 300 K and results for three different charge carrier concentrations are compared. (a), (b) refer to electron doping, while (c), (d) refer to hole doping. The electronic part  $\kappa_{el}$  was calculated, while the lattice part  $\kappa_{ph}$  was taken from literature<sup>8,12</sup>. As a reference point experimental results for the mixed single crystal series  $(\text{Bi}_x\text{Sb}_{1-x})_2\text{Te}_3$  at comparable material composition are shown as green downward triangles<sup>64</sup>.

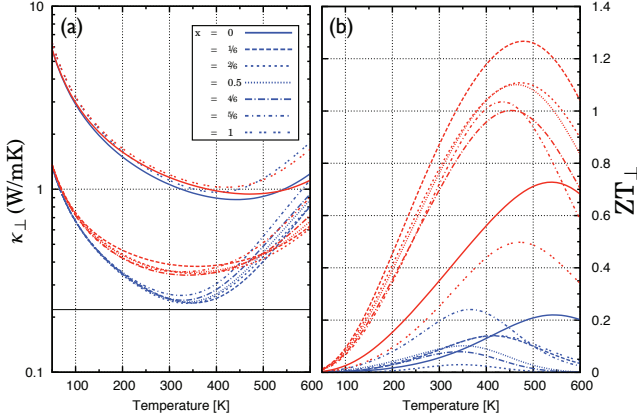


FIG. 9. (color online) Temperature dependence of the thermal conductivity and figure of merit for the  $(\text{Bi}_2\text{Te}_3)_x/(\text{Sb}_2\text{Te}_3)_{1-x}$  SLs. Shown are (a) total cross-plane thermal conductivity  $\kappa_{\perp} = \kappa_{el,\perp} + \kappa_{ph,\perp}$  and (b) cross-plane figure of merit. The charge carrier concentration is fixed to  $N = 3 \times 10^{19} \text{ cm}^{-3}$  and different line types correspond to different SL periods. Blue lines refer to electron doping, while red lines refer to hole doping. The electronic part  $\kappa_{el}$  was calculated, while the lattice part  $\kappa_{ph}$  was taken from literature<sup>8,12</sup>.

$N = 9 \times 10^{19} \text{ cm}^{-3}$  for  $\text{Sb}_2\text{Te}_3$ . One easily abstracts that  $ZT_{\perp}$  values of the optimal doped SLs and the mixed single crystal series show clear similarities considering the dependence on the materials composition, as well as the absolute values of  $ZT_{\perp}$ .

To extend our findings at room-temperature, in Figure 9(a) and (b) temperature dependent results for the total

cross-plane thermal conductivity and cross-plane FOM are shown for the  $(\text{Bi}_2\text{Te}_3)_x/(\text{Sb}_2\text{Te}_3)_{1-x}$  SLs at electron/hole concentration of  $N = 3 \times 10^{19} \text{ cm}^{-3}$ . Within, a conventional  $1/T$  dependence for the lattice thermal conductivity was assumed<sup>83</sup>, while the calculated electronic part  $\kappa_{el}$  is temperature and doping dependent, per se. We note that for thermoelectric SLs no clear tendency on the temperature dependence of  $\kappa_{ph}$  can be revealed. However, conventional  $1/T$  dependence, as well as temperature independent  $\kappa_{ph}$  were found experimentally<sup>72,73,84</sup>. Models show, that  $\kappa_{ph}$  should diminish at low periods<sup>85</sup>, while experiments reveal a saturation towards the alloy limit for SL periods below  $50 \text{ \AA}$ <sup>8</sup>.

As can be seen from Figure 9(a)  $\kappa_{\perp}$  takes a minimum at about 300 – 400 K for the  $\text{Bi}_2\text{Te}_3/\text{Sb}_2\text{Te}_3$  SLs. This behaviour is dictated by the electronic contribution to  $\kappa_{\perp}$  and supported by the  $1/T$  dependence of the lattice part of  $\kappa$ . At low temperature the chemical potential is located in the bands and thus a moderate contribution to  $\kappa_{el,\perp}$  is obtained. With increasing temperature  $\kappa_{el,\perp}$  slightly decreases as the chemical potential shifts towards the band edges, then reaching minimal  $\kappa_{el,\perp}$  for chemical potential positions at the band edges (cf. Figure 7). At elevated temperatures the bipolar contribution leads to an enhanced electronic contribution to  $\kappa_{\perp}$ , which then clearly dominates the  $1/T$  dependence of the lattice part of  $\kappa$  leading to large values of the total thermal conductivity. The influence of the electronic contribution is more pronounced in the SLs compared to bulk, as here  $\kappa_{el,\perp} \geq \kappa_{ph,\perp}$ . Combining these results with the temperature dependent power factor  $\text{PF}_{\perp}$  discussed in Figure 5(d) we find the temperature dependence on the cross-plane FOM as presented in Figure

9(b). Concentrating on the more promising p-type SLs we state maximized values for  $ZT_{\perp}$  clearly above unity for temperatures of 400 – 500 K. The largest cross-plane FOM is found to be  $ZT_{\perp} = 1.27$  at about 470 K for a  $(\text{Bi}_2\text{Te}_3)_x/(\text{Sb}_2\text{Te}_3)_{1-x}$  SL at  $x = 1/6$  and a hole concentration of  $N = 3 \times 10^{19} \text{ cm}^{-3}$ . We want to mention that in the experiments of Ref. 12 the maximal  $ZT_{\perp}$  under hole doping was stated at a SL period of  $x = 1/6$ , too. The best value for an n-type SL is  $ZT_{\perp} = 0.25$  at about 360 K at a SL period of  $x = 5/6$ .

## V. CONCLUSION

The anisotropic thermoelectric transport properties of  $\text{Bi}_2\text{Te}_3/\text{Sb}_2\text{Te}_3$  superlattices at different superlattice periods is presented to get insight into the physical mechanisms which are responsible for the path-breaking experimental results with  $ZT_{\perp} = 2.4$  at room temperature obtained by Ref. 12. Several aspects added up to obtain those very high ZT values in experiment. (i) In-plane values of the electrical conductivity and thermopower were found to be larger than in the bulk systems at comparable charge carrier concentrations. (ii) An elimination of the electrical conductivity anisotropy  $\sigma_{\parallel}/\sigma_{\perp}$ , which is apparent in both bulk systems, was found in superlattices at certain periods. (iii) The lattice part of the thermal conductivity was reduced below the alloy limit due to phonon-blocking at the superlattice interfaces<sup>8,24</sup>.

Even though taking into account the most optimistic value  $\kappa_{ph,\perp} = 0.22 \text{ W/mK}$  for the lattice part of the thermal conductivity, we found the cross-plane figure of merit for the best p-type superlattice to be  $ZT_{\perp} = 0.9$  at room temperature and slightly enhanced to  $ZT_{\perp} = 1.27$  at elevated temperature. However, this is more than a factor of

two worse than experimentally revealed and is caused by the fact, that within the presented *ab initio* calculations the findings (i) and (ii) could not be confirmed. We want to add, that in first consistent experiments by Venkatasubramanian *et al.*<sup>62</sup> a room-temperature  $ZT_{\perp} = 1.2$  was proposed for a non-symmetrical  $\text{Bi}_2\text{Te}_3/\text{Sb}_2\text{Te}_3$  superlattice with a period of 30 Å.

For the in-plane transport properties of S,  $\sigma$  and PF we can state values comparable to bulk for the p-type and n-type superlattices, which is in agreement to recent experiments<sup>21,26</sup>. Furthermore for the p-type superlattices a conservation of the bulk transport anisotropies is found, but in no case a reduction, while under electron doping strong quantum well effects due to conduction band offsets lead to large transport anisotropies  $\sigma_{\parallel}/\sigma_{\perp} \geq 10$  and suppress the cross-plane thermoelectric transport notably.

Concluding, the experimentally found remarkable thermoelectric transport properties in  $\text{Bi}_2\text{Te}_3/\text{Sb}_2\text{Te}_3$  superlattices could not be revealed by detailed band structure effects. An ongoing issue will be to clarify, whether scattering effects caused by defects and lattice imperfections could give a considerable leap forward to understand the enhanced thermoelectric efficiency in  $\text{Bi}_2\text{Te}_3/\text{Sb}_2\text{Te}_3$  superlattices.

## ACKNOWLEDGMENTS

This work was supported by the Deutsche Forschungsgemeinschaft, SPP 1386 ‘Nanostrukturierte Thermoelektrika: Theorie, Modellsysteme und kontrollierte Synthese’. N. F. Hinsche is member of the International Max Planck Research School for Science and Technology of Nanostructures.

---

\* [nicki.hinsche@physik.uni-halle.de](mailto:nicki.hinsche@physik.uni-halle.de)

<sup>1</sup> G. J. Snyder and E. Toberer, *Nature Materials*, **7**, 105 (2008).

<sup>2</sup> C. J. Vineis, A. Shakouri, A. Majumdar, and M. G. Kanatzidis, *Advanced Materials*, **22**, 3970 (2010).

<sup>3</sup> D. A. Wright, *Nature*, **181**, 834 (1958).

<sup>4</sup> T. Caillat, M. Carle, P. Pierrat, H. Scherrer, and S. Scherrer, *Journal of Physics and Chemistry of Solids*, **53**, 1121 (1992).

<sup>5</sup> B. Poudel, Q. Hao, Y. Ma, Y. Lan, A. Minnich, B. Yu, X. Yan, D. Wang, A. Muto, and D. Vashaee, *Science*, **320**, 634 (2008).

<sup>6</sup> G. Slack, “New materials and performance limits for thermoelectric cooling,” in *CRC Handbook of Thermoelectrics*, edited by D. M. Rowe (CRC Press, Boca Raton, 1995) Chap. 34.

<sup>7</sup> G. Chen, *Physical Review B*, **57**, 14958 (1998).

<sup>8</sup> R. Venkatasubramanian, *Phys. Rev. B*, **61**, 3091 (2000).

<sup>9</sup> T. Koga, X. Sun, S. Cronin, and M. Dresselhaus, in 18th International conference on thermoelectrics (1999) pp. 378–381; *Applied Physics Letters*, **75**, 2438 (1999);

T. Koga, T. Harman, S. Cronin, and M. Dresselhaus, *Phys. Rev. B*, **60**, 14286 (1999); T. Koga, S. Cronin, M. Dresselhaus, and J. Liu, *Applied Physics Letters*, **77**, 1490 (2000).

<sup>10</sup> H. Böttner, G. Chen, and R. Venkatasubramanian, *MRS bulletin*, **31**, 211 (2006).

<sup>11</sup> R. Venkatasubramanian, T. Colpitts, B. O’Quinn, S. Liu, N. El-Masry, and M. Lamvik, *Applied Physics Letters*, **75**, 1104 (1999).

<sup>12</sup> R. Venkatasubramanian, E. Siivola, and T. Colpitts, *Nature*, **413**, 597 (2001).

<sup>13</sup> A. Majumdar, *Science*, **303**, 777 (2004).

<sup>14</sup> R. Delves, A. Bowley, and D. Hazelden, *Proceedings of the Phys. Society*, **78**, 838 (1961).

<sup>15</sup> M. Stordeur and W. Heiliger, *physica status solidi (b)*, **78**, K103 (1976).

<sup>16</sup> M. Stordeur and W. Kühnberger, *physica status solidi (b)*, **69**, 377 (1975).

<sup>17</sup> B. Huang and M. Kaviani, *Phys. Rev. B*, **77**, 125209 (2008).

<sup>18</sup> N. Hinsche, B. Yavorsky, I. Mertig, and P. Zahn, *Physical*



- Review B, **84**, 165214 (2011).
- <sup>19</sup> H. Beyer, J. Nurnus, H. Böttner, A. Lambrecht, E. Wagner, and G. Bauer, *Physica E: Low-dimensional Systems and Nanostructures*, **13**, 965 (2002).
  - <sup>20</sup> H. Böttner, J. Nurnus, A. Gavrikov, and G. Kuhner, *Journal of microelectromechanical systems*, **13**, 414 (2004).
  - <sup>21</sup> J. König, M. Winkler, S. Buller, W. Bensch, U. Schürmann, L. Kienle, and H. Böttner, *Journal of Electronic Materials*, **40**, 1266 (2011).
  - <sup>22</sup> C.-N. Liao, C.-Y. Chang, and H.-S. Chu, *Journal of Applied Physics*, **107**, 066103 (2010).
  - <sup>23</sup> N. Peranio, O. Eibl, and J. Nurnus, *Journal of Applied Physics*, **100**, 114306 (2006).
  - <sup>24</sup> M. N. Touzelbaev, P. Zhou, R. Venkatasubramanian, and K. E. Goodson, *Journal of Applied Physics*, **90**, 763 (2010).
  - <sup>25</sup> N. Peranio, M. Winkler, Z. Aabdin, J. König, H. Böttner, and O. Eibl, *physica status solidi (a)*, **209**, 289 (2011).
  - <sup>26</sup> M. Winkler, X. Liu, J. König, L. Kirste, H. Böttner, W. Bensch, and L. Kienle, *Journal of Electronic Materials*, **41**, 1322 (2012).
  - <sup>27</sup> T. Scheidemantel, C. Ambrosch-Draxl, T. Thonhauser, J. Badding, and J. Sofo, *Physical Review B*, **68**, 125210 (2003).
  - <sup>28</sup> T. Thonhauser, T. Scheidemantel, J. Sofo, J. Badding, and G. Mahan, *Physical Review B*, **68**, 085201 (2003).
  - <sup>29</sup> G. Wang and T. Cagin, *Physical Review B*, **76**, 075201 (2007).
  - <sup>30</sup> G. Wang and T. Cagin, *Applied Physics Letters*, **89**, 152101 (2006).
  - <sup>31</sup> M. S. Park, J.-H. Song, J. E. Medvedeva, M. Kim, I. G. Kim, and A. J. Freeman, *Phys. Rev. B*, **81**, 155211 (2010).
  - <sup>32</sup> H. Li, D. Bilc, and S. D. Mahanti, *Mat. Res. Soc. Symp. Proc.*, **793**, 837 (2004).
  - <sup>33</sup> O. Madelung, M. Schulz, and H. Weiss, eds., “Landolt-börnstein new series, group iii/41c,” in *Numerical Data and Functional Relationship in Science and Technology* (Springer Verlag, Berlin, 1998).
  - <sup>34</sup> B. Y. Yavorsky, N. Hinsche, I. Mertig, and P. Zahn, *Physical Review B*, **84**, 165208 (2011).
  - <sup>35</sup> M. Gradhand, M. Czerner, D. V. Fedorov, P. Zahn, B. Y. Yavorsky, L. Szunyogh, and I. Mertig, *Phys. Rev. B*, **80**, 224413 (2009).
  - <sup>36</sup> S. H. Vosko and L. Wilk, *Phys. Rev. B*, **22**, 3812 (1980).
  - <sup>37</sup> I. Mertig, *Reports on Progress in Physics*, **62**, 237 (1999).
  - <sup>38</sup> N. Hinsche, I. Mertig, and P. Zahn, *J. Phys.: Condens. Matter*, **23**, 295502 (2011).
  - <sup>39</sup> D. J. Singh, *Physical Review B*, **81**, 195217 (2010).
  - <sup>40</sup> D. Parker and D. J. Singh, *Physical Review B*, **82**, 035204 (2010).
  - <sup>41</sup> A. May, D. J. Singh, and G. J. Snyder, *Physical Review B*, **79**, 153101 (2009).
  - <sup>42</sup> M.-S. Lee, F. Poudeu, and S. Mahanti, *Physical Review B*, **83**, 085204 (2011).
  - <sup>43</sup> S. Lee and P. von Allmen, *Applied Physics Letters*, **88**, 022107 (2006).
  - <sup>44</sup> M. Situmorang and H. Goldsmid, *physica status solidi (b)*, **134**, K83 (1986).
  - <sup>45</sup> T. Thonhauser, *Solid State Communications*, **129**, 249 (2004).
  - <sup>46</sup> G. Mahan and J. Sofo, *Proceedings of the National Academy of Sciences*, **93**, 7436 (1996).
  - <sup>47</sup> P. Zahn, N. Hinsche, B. Yavorsky, and I. Mertig, *J. Phys.: Condens. Matter*, **23**, 505504 (2011).
  - <sup>48</sup> G. Nolas and H. Goldsmid, “Thermal conductivity of semiconductors,” in *Thermal conductivity: theory, properties, and applications*, edited by T. Tritt (Kluwer Academic, New York, 2004) Chap. 1.4.
  - <sup>49</sup> R. Sehr, *Journal of Physics and Chemistry of Solids*, **23**, 1219 (1962).
  - <sup>50</sup> G. Lehmann and M. Taut, *physica status solidi (b)*, **54**, 469 (1972).
  - <sup>51</sup> I. Mertig, E. Mrosan, and P. Ziesche, *Multiple scattering theory of point defects in metals: Electronic properties* (B.G. Teubner, Leipzig, 1987).
  - <sup>52</sup> P. Mori-Sánchez, A. Cohen, and W. Yang, *Phys. Rev. Lett.*, **100**, 146401 (2008).
  - <sup>53</sup> Y. Varshni, *Physica*, **34**, 149 (1967).
  - <sup>54</sup> A. von Middendorff, K. Dietrich, and G. Landwehr, *Solid State Communications*, **13**, 443 (1973).
  - <sup>55</sup> H. Zhang, C. Liu, X. Qi, X. Dai, Z. Fang, and S. Zhang, *Nature Physics*, **5**, 438 (2009).
  - <sup>56</sup> O. Yazyev, E. Kioupakis, J. Moore, and S. Louie, *Physical Review B*, **85**, 161101 (2012).
  - <sup>57</sup> H. Jeon, H. Ha, D. Hyun, and J. Shim, *Journal of Physics and Chemistry of Solids*, **52**, 579 (1991).
  - <sup>58</sup> D. M. Rowe, ed., *CRC Handbook of Thermoelectrics* (CRC Press, Boca Raton, 1995).
  - <sup>59</sup> H. Scherrer and S. Scherrer, “Valence band structure and the thermoelectric figure-of-merit of (bil-xsbx)2te3 crystals,” in *CRC Handbook of Thermoelectrics*, edited by D. M. Rowe (CRC Press, Boca Raton, 1995) Chap. 19.
  - <sup>60</sup> We note, that no coherent data of  $N$ ,  $\sigma_{\parallel}$ ,  $S_{\parallel}$  and  $PF_{\parallel}$  for the SL is available.  $N$  and  $\sigma_{\parallel}$  were concluded from Ref. 12, while  $S_{\parallel}$  was estimated from Refs. 61–63 for comparable SLs, but most probably not from the same sample.
  - <sup>61</sup> R. Venkatasubramanian, T. Colpitts, E. Watko, M. Lamvik, and N. El-Masry, *Journal of crystal growth*, **170**, 817 (1997).
  - <sup>62</sup> R. Venkatasubramanian, T. Colpitts, E. Watko, and J. Hutchby, *Fifteenth International Conference on Thermoelectrics*, 454 (1996).
  - <sup>63</sup> R. Venkatasubramanian, *Bi2Te3/Sb2Te3 Superlattice Structures for HTE*, Tech. Rep. (Office of Naval Research, USA, 1997).
  - <sup>64</sup> M. Stordeur, “Bismuth telluride, antimony telluride, and their solid solutions,” in *CRC Handbook of Thermoelectrics*, edited by D. M. Rowe (CRC Press, Boca Raton, 1995) Chap. 20.
  - <sup>65</sup> L. Hicks, T. Harman, and M. Dresselhaus, *Applied Physics Letters*, **63**, 3230 (1993); L. Hicks and M. Dresselhaus, *Physical Review B*, **47**, 12727 (1993).
  - <sup>66</sup> M. Dresselhaus, G. Dresselhaus, X. Sun, Z. Zhang, S. Cronin, and T. Koga, *Phys. Solid State*, **41**, 679 (1999).
  - <sup>67</sup> J. Sofo and G. Mahan, *AIP Conference Proceedings*, **316**, 239 (1994).
  - <sup>68</sup> D. Broido and T. Reinecke, *Physical Review B*, **51**, 13797 (1995).
  - <sup>69</sup> S. Eremeev, G. Landolt, T. Menshchikova, B. Slomski, Y. Koroteev, Z. Aliev, M. Babanly, J. Henk, A. Ernst, and L. Patthey, *Nature Communications*, **3**, 635 (2012).
  - <sup>70</sup> J. Sootsman, D. Chung, and M. Kanatzidis, *Angewandte Chemie*, **121**, 8768 (2009).
  - <sup>71</sup> P. Zahn, J. Binder, I. Mertig, R. Zeller, and P. Dederichs, *Phys. Rev. Lett.*, **80**, 4309 (1998).
  - <sup>72</sup> S. Lee, D. Cahill, and R. Venkatasubramanian, *Appl. Phys. Lett.*, **70**, 2957 (1997).
  - <sup>73</sup> T. Borca-Tasciuc, W. Liu, J. Liu, T. Zeng, D. W. Song, C. D. Moore, G. Chen, K. L. Wang, M. S. Goorsky,

- T. Radetic, R. Gronsky, T. Koga, and M. S. Dresselhaus, *Superlattices and Microstructures*, **28**, 199 (2000).
- <sup>74</sup> S. Huxtable, A. Abramson, and C. Tien, *Applied Physics Letters*, **80**, 1737 (2002).
- <sup>75</sup> S. Chakraborty, C. Kleint, A. Heinrich, C. Schneider, J. Schumann, M. Falke, and S. Teichert, *Applied Physics Letters*, **83**, 4184 (2003).
- <sup>76</sup> H. Goldsmid, *Advances in Physics*, **14**, 273 (1965).
- <sup>77</sup> H. Fröhlich and C. Kittel, *Physica*, **3**, 1086 (1954).
- <sup>78</sup> C. Uher and H. Goldsmid, *Phys Status Solidi B*, **65**, 765 (1974).
- <sup>79</sup> H. Goldsmid, *Proceedings of the Physical Society. Section B*, **69**, 203 (1956).
- <sup>80</sup> L. Chaput, P. Pêcheur, J. Tobola, and H. Scherrer, *Phys. Rev. B*, **72**, 085126 (2005).
- <sup>81</sup> N. F. Hinsche, I. Mertig, and P. Zahn, (2012), [arXiv:0000.0000 \[cond-mat.mes-hall\]](https://arxiv.org/abs/0000.0000).
- <sup>82</sup> We want to mention that the lattice thermal conductivity was found to be a function of the SL period<sup>8</sup>. As a lack of further data, we assumed the smallest  $\kappa_{ph,\perp}$  for all of our SL periods.
- <sup>83</sup> N. Peranio, Structural, chemical, and thermoelectric properties of Bi<sub>2</sub>T Ph.D. thesis, Eberhard-Karls-Universität zu Tübingen (2008).
- <sup>84</sup> M. Hase and J. Tominaga, *Applied Physics Letters*, **99**, 031902 (2011).
- <sup>85</sup> A. Pattamatta and C. K. Madnia, *Int J Heat Mass Tran*, **52**, 860 (2009).